ELSEVIER Solar Energy Materials and Solar Cells 53 (1998) 367–377

Solar Energy Materials & Solar Cells

Blue-photon modification of nonstandard diode barrier in $CuInSe_2$ solar cells

I.L. Eisgruber[a,*], J.E. Granata[a], J.R. Sites[a], J. Hou[b], J. Kessler[1c]

[a] *Physics Department, Colorado State University, Fort Collins, CO 80523, USA*
[b] *Electronic Materials and Processing Research Laboratory, Pennsylvania State University, State College, PA 16801 USA*
[c] *Solarex, 826 Newtown-Yardley Road, Newtown, Pennsylvania, PA 18940, USA*

Received 2 October 1997

Abstract

The current–voltage curves of many ZnO/CdS/$CuInSe_2$ solar cells display significant distortion when only red light illumination is employed. This distortion generally disappears or partially disappears for a period of time following illumination with blue light. Similarly, the dark diode curve shortly after illumination containing blue light is shifted significantly from the equilibrium dark curve. This effect is more common than generally realized and indicates a mechanism that is potentially detrimental to photovoltaic efficiency. A model is presented that is based on a low free-electron concentration and a high concentration of deep levels in the CdS window layer. This model is consistent with observed variations in current–voltage, capacitance, and laser scan data with illumination wavelength and history.

Keywords: $CuInSe_2$; Thin film; Current-voltage

1. Introduction

$CuInSe_2$ (CIS) and alloys where Ga is partially substituted for In are promising materials for low-cost thin-film polycrystalline solar cells. Efficiencies near or

* Corresponding address: Materials Research Group; 12441 W. 49th Ave., Suite #2; Wheat Ridge, CO 80033-1927, USA. E-mail: supervacuo@aol.com

[1] Current address: Uppsala University; Angstrom Laboratory; Solid State Electronics; S-751 21 UPPSALA; Sweden.

0927-0248/98/$19.00
PII S0927-0248(98)00035-X

exceeding 17% have been demonstrated both in the US [1,2] and in Europe [3]. An understanding of the electrical behavior of these cells, and how processing techniques affect this behavior, is integral to upscaling from small area devices to commercial modules within the framework of acceptable production costs. At Solarex [4,5], in an effort to transfer the experience from high-quality, small-area device fabrication to (sub)module fabrication, a number of "reasonably" efficient CIS cells have shown current–voltage (I–V) curves that differ significantly under red illumination from the "standard" exponential curve with a photocurrent displacement.

This paper describes the characteristics of cells showing the unusual red light, and corresponding dark, current–voltage response, and it proposes a model to explain these characteristics. The measured characteristics include I–V curves as a function of time, illumination wavelength, and illumination history; capacitance as a function of illumination history; and uniformity of laser scanning response [6] as a function of illumination wavelength and illumination history. ADEPT software developed at Purdue University [7] and AMPS from Pennsylvania State University [8] are used to calculate the energy band structure and resulting I–V curves for the proposed device structures.

2. Cell behavior

Fig. 1a shows the typical form of the red I–V curve, the reversion to a standard exponential curve following exposure to light containing short-wavelength photons, and the corresponding shift in the dark diode curve to lower voltage. For cells produced from identical CIS and ZnO layers, it has been observed that the existence of the distortion in the red curve is related to the type of chemical bath process used for the CdS buffer layer formation. When the distortion is present, its details vary from cell to cell, and in some cases, partial distortion remains even under white-light illumination. The distortion in the red light I–V curve disappears when the device is exposed to white light, but the distortion will reappear gradually after the white light is removed. Fig. 1b shows the typical recovery of the red-light distortion following white-light illumination. The time constants involved span the range from a few minutes to a few hours.

The wavelengths necessary to induce a change in the I–V curves are determined from Fig. 2. The voltage shift ΔV for the dark curves is the voltage difference at $+5\ \mathrm{mA/cm^2}$ before and after the cell is exposed to illumination of the wavelength shown. For wavelengths of 600 nm and above, there is no change. For 500 nm and below, the shift is similar to that depicted in Fig. 1a. The voltage shift ΔV for the monochromatic light curves is the voltage difference at $-5\ \mathrm{mA/cm^2}$ before and after the exposure to white light. There is a significant shift for wavelengths of 600 nm and above. For 500 nm and below, which presumably induces the same effect as the white light, there is a small shift in the opposite direction, but much smaller in magnitude. Within experimental error, the boundary between short-wavelength ("blue") and long-wavelength ("red") response is the band gap of CdS.

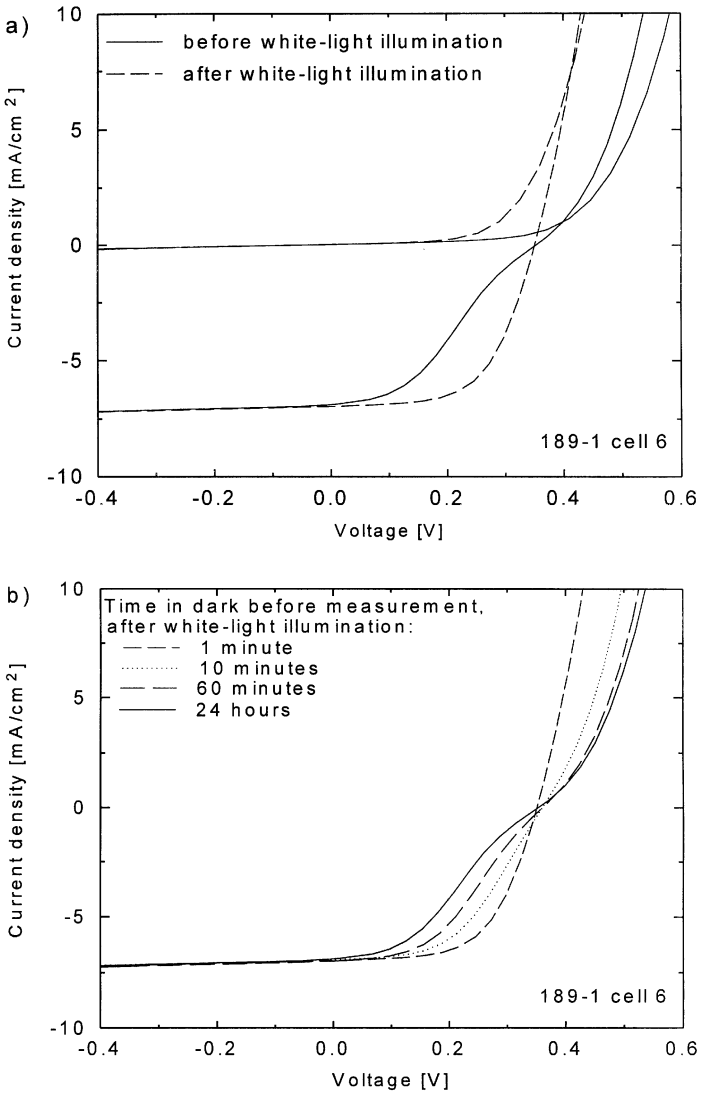

Fig. 1. (a) Dark and red-light current–voltage characteristics before and after white-light illumination. (b) Red-light current–voltage characteristics as a function of time after white-light illumination.

The magnitude of the *I–V* distortion may vary from cell to cell or even over the surface of an individual cell. Fig. 3 shows red and dark *I–V* curves for a second cell. The distortion shows the same qualitative behavior as that seen in Fig. 1a, but the voltage magnitude of the distortion is much larger. In fact, in Fig. 3, the distortion is large enough to extend across the zero voltage bias axis, reducing the cell's red short-circuit current.

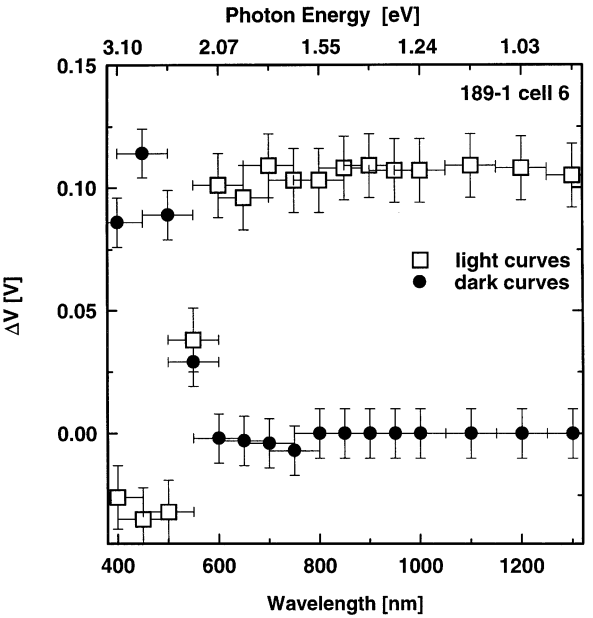

Fig. 2. Voltage shift in dark curve after monochromatic illumination of the indicated wavelength, and in monochromatic I–V curves of different wavelengths after white illumination.

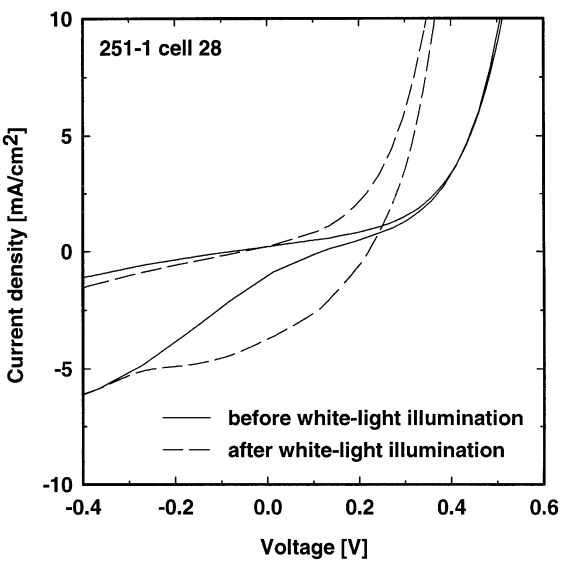

Fig. 3. Dark and red-light current–voltage characteristics before and after white-light illumination for a cell with large red-light distortion.

Fig. 4 illustrates the variation of the distortion over the surface of several cells, including (upper left cell) that depicted in Fig. 3. The figure shows a short-circuit red (633 nm) laser scan for six cells on a common substrate. The lighter regions are those of higher red short-circuit current, and the darker ones show lower red short-circuit current. The thick dark areas are the probe shadows, and the straight lines are the cell grid fingers. The red short-circuit current varies by a factor of four over the cell layout shown, corresponding to local quantum efficiencies ranging from 20% in parts of the lower left cell to 80% at the top of the upper cells. Also note that there are islands of high response in the lower left cell. These islands would not be present if the low response were due to other mechanisms such as excessive shunting defects [9]. The IV curves of Fig. 3 were measured on the upper left cell in the laser scan of Fig. 4.

Fig. 5 shows the contrast between red (upper left) and blue (lower left) scans for a single cell. The blue scan corresponds to a quantum efficiency uniformly near 80%.

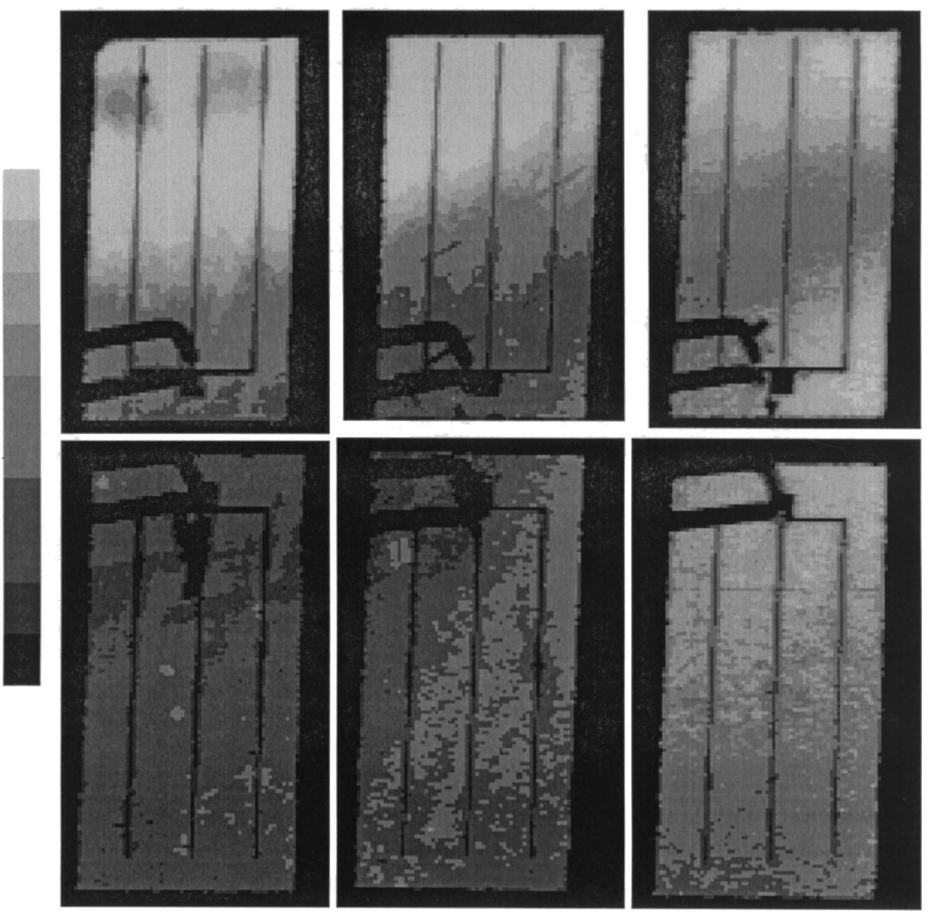

Fig. 4. Red laser scan of six adjacent cells.

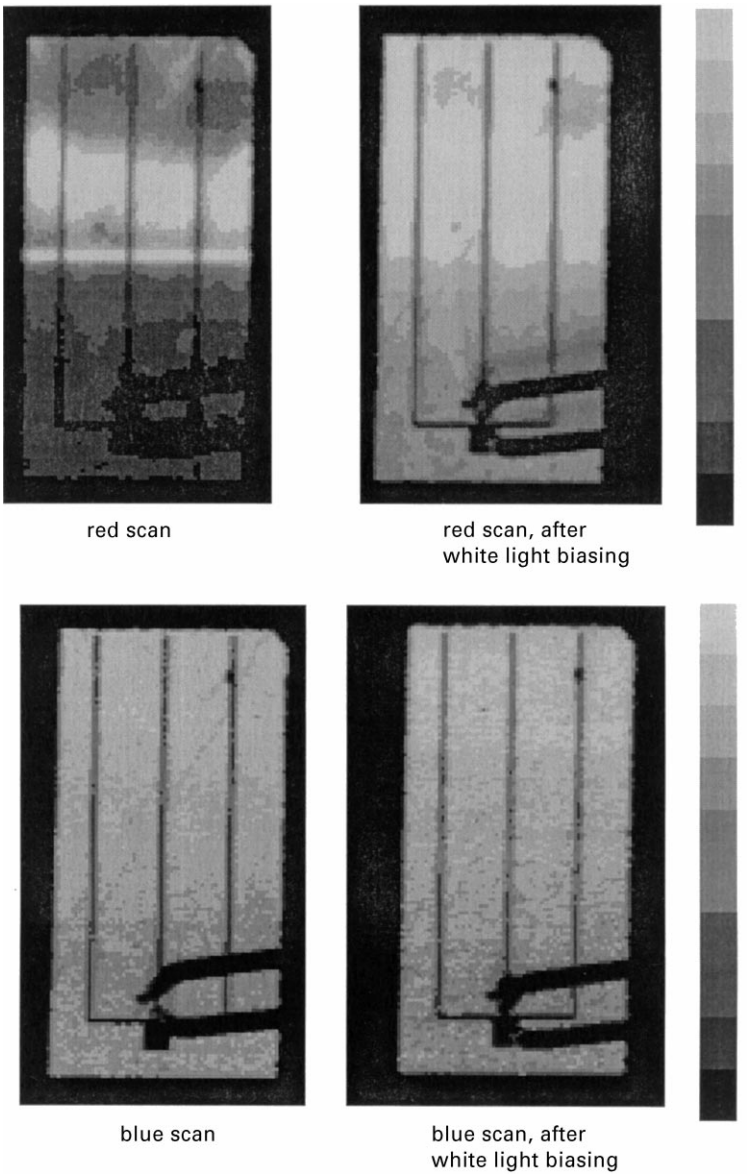

Fig. 5. Large-scale laser scans using red and blue lasers, before and after white-light illumination.

Also shown are the red and blue scans after exposure to white light. The red scan has become more uniform with local quantum efficiencies approaching the blue-light QE values. The blue scan is essentially unchanged. There is, incidentally, a line of high response in the initial red scan at the upper left. This line is due to inadvertent exposure by a single-line blue scan shortly before the red scan was made.

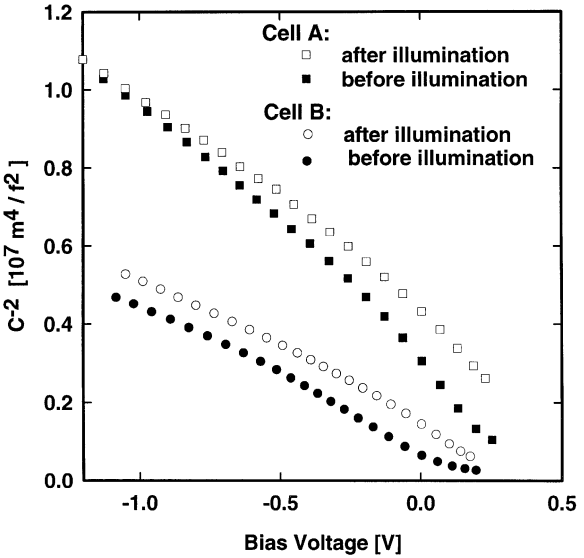

Fig. 6. Capacitance data ($f = 50$ kHz) before and after illumination for two cells.

A final probe of the effect of blue photons on diode electronics is shown in Fig. 6, which compares dark capacitance before and immediately after white light illumination for two cells. The frequency dependence is quite flat between 10 and 100 kHz. One of the cells has an initial carrier density higher than the other, as deduced from the C^{-2} vs. V slopes, but in both cases there is a clear shift to smaller capacitance, or a greater depletion width and lower carrier density, following the illumination [10].

3. Explanation and modeling

Two general features appear to be required for a solar-cell model to reproduce the observed distortion in the J–V curves: (i) a sign reversal in the conduction-band slope such as that resulting from a CdS/CIS band offset, and (ii) CdS doping sufficiently small and thickness sufficiently wide that the sign reversal occurs at conduction-band energies approaching the bulk CIS level. In addition, removal of the J–V distortion by blue light requires (iii) long-lived deep-level acceptor states in the CdS at a concentration comparable to its donor density. Fig. 7a shows sample band diagrams for ZnO/CdS/CIS cells. Layer thicknesses are typical values used in the Solarex processes. The conduction-band offsets shown are taken from the recent experimental [11] and theoretical [12] determinations, all of which have an uncertainty of at least 0.1 eV. The carrier concentrations for the ZnO as well as the CIS and its In-rich surface layer are chosen from a realistic range and are consistent with capacitance measurements. Two situations for the equilibrium CdS carrier concentration are distinguished. Either

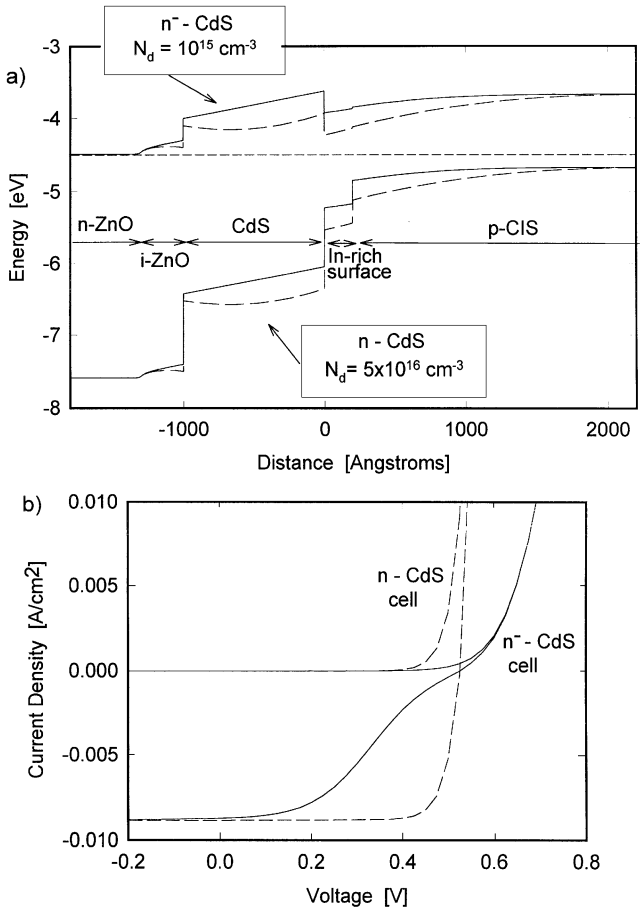

Fig. 7. (a) Energy band diagrams for CIS cells with n^--CdS and n-CdS. (b) Calculated light and dark IV curves for n^--CdS and n-CdS cells. Solid lines show the n^--CdS case, and dashed lines show the n-CdS case.

it is low (referred to as the n^--CdS case), or it is not low (referred to as the n-CdS case). In the n^--CdS case, the CdS creates a barrier with a peak approaching the bulk CIS conduction band edge. In the n-CdS case, the CdS barrier maximum is much lower in energy.

Fig. 7b shows the simulated I–V characteristics for the two-band structures calculated with ADEPT software. The critical parameters are the CdS/CIS conduction band offset, the CdS carrier density, and the CdS thickness. Under illumination, the n^--CdS barrier partially blocks the photocurrent generated in the absorber when the cell is in sufficient forward bias. This type of barrier produces the red-light distortion. The n^--CdS barrier also acts as a block to forward current, and hence the n^--CdS cell exhibits reduced magnitude forward currents both above and below V_{oc}. The n-CdS

barrier, however, does not significantly block the currents. Comparison of these calculated I–V curves to Fig. 1a shows that the measured cell behavior before white-light illumination is very similar to that of the n^--CdS case, and the measured cell behavior after white light illumination is similar to that of the n-CdS case. The calculated behavior varies somewhat with the choice of material parameters and layer thicknesses, but the qualitative features of Figs. 1 and 7b are present over a significant range of parameters. Thicker CdS or lower CdS carrier concentration increases the magnitude of the red-light distortion, and can simulate the larger-distortion I–V curves of Fig. 3.

The change in experimental I–V curves with exposure to blue photons is explained as a modification in the occupation of deep CdS states. Fig. 8a shows n-CdS without deep levels, where the n-type behavior is due to ionization of shallow donor states. The n^--CdS case is attributed to a density of acceptor-like deep states comparable to

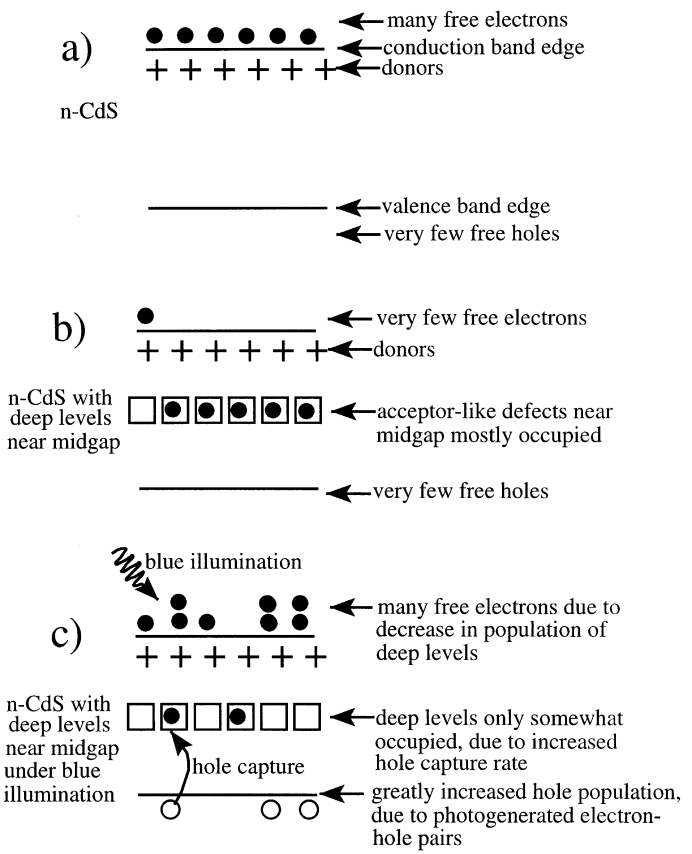

Fig. 8. Carrier populations in (a) n-type CdS (b) n-type CdS with deep levels, and (c) n-type CdS with deep levels under blue illumination

the donor density. These deep acceptor states trap most of the free electrons contributed by the donors. The resulting low free electron concentration is shown in Fig. 8b. When incident blue photons are absorbed in the CdS, the concentrations of both free electrons and free holes increase greatly, and many of the deep levels are now occupied by light-generated holes, as shown in Fig. 8c. If these deep levels are long-lived, the CdS will remain in the 8c configuration for an extended time, and one will have effectively photoinduced a transition from n^--CdS (few free electrons) to n-CdS (many free electrons). The long relaxation times observed after the illumination is removed (Fig. 1b), can be attributed to the slow discharging of the deep traps. Furthermore, the necessity to have photons with energy greater than the CdS band gap is clearly verified by the Fig. 2 data.

It appears that the specific experimental features can be explained by a low free carrier concentration and high deep level density in the CdS layer. The local variations in Fig. 4 likely correspond to regions of slightly different compensation levels, as simulations indicate that a 25% change in trap density can produce a factor of four variation in laser scan signal. Finally, Fig. 7a shows an increase in depletion width of about 10% between the n and n-structure, which is consistent with the capacitance decrease (C^{-2} increase) shown in Fig. 6.

4. Discussion

The simple model of a ZnO/CdS/CIS cell with a significant deep-level density and low free carrier concentration in the CdS explains the experimentally observed cell features. The red light curve exhibits a significant distortion that disappears under illumination by photons with energy greater than the CdS band gap. The existence of the distortion primarily depends on the thickness and free electron density of the CdS. The long relaxation time is due to the slow discharge rate of the deep states.

It is a reasonable assumption that there are a number of CIS cells being fabricated that exhibit at least a small I–V distortion, but are not recognized as such, because it is not routine to measure red-light I–V characteristics. In fact there are numerous CIS I–V curves that fail to exhibit light–dark I–V superposition, and a likely explanation is that a dark curve distorted toward higher voltages is compared with a white-light curve where the distortion has been removed. The impact of the effect on cell efficiency and characterization techniques may be more widespread than generally realized. A practical recommendation for those developing CIS solar cells is to be alert to distortions in light I–V curves, or unexplained light–dark nonsuperposition, and follow up in such cases with red-only I–V measurements.

Acknowledgements

The authors gratefully acknowledge Jeffrey Gray of Purdue University and Xiao Xiang Liu of Colorado State University for assistance with ADEPT simulations, Rick Matson of the National Renewable Energy Laboratory for use of the large-scale laser

scanner, and Sally Asher of the National Renewable Energy Laboratory. The research performed at CSU and Solarex is supported by the National Renewable Energy Laboratory, and the research performed at PSU was supported by the Electric Power Research Institute.

References

[1] A.M. Gabor, J.R. Tuttle, D.S. Albin, A.L. Tennant, M.A. Contreras, R. Noufi, A.M. Hermann, AIP Conf. Proc. vol. 306 1993, p. 59.
[2] J.R. Tuttle, M.A. Contreras, J.S. Ward, A.M. Gabor, K.R. Ramanathan, A.L. Tennant, L. Wang, J. Keane, R. Noufi, High-efficiency Cu(ln,Ga)se_2-based thin-film solar cells: 16.8% total-area 1-sun and 17.2% total-area 22-sun device performance, Proc. 1st World Conf. on Photovoltaic Energy Conversion, 1994, pp. 1942–1945.
[3] J. Hedstrom, H. Ohlsen, M. Bodegard, A. Kylner, L. Stolt, D. Hariskos, M. Ruckh, H. Schock, Zn0/CdS/Cu(In,Ga)Se_2 Thin film solar cells with improved performance, Proc. 23rd IEEE Photovoltaics Specialists Conf., 1993, pp. 364–371.
[4] J. Kessler, S. Wiedeman, L. Russell, T. Lommasson, S. Skibo, J. Foglebach, T. Kloss, R.R. Arya, Progress in Cu(In,Ga)Se_2 solar cells and submodules, Proc. 1st World Conf. on Photovoltaic Energy Conversion, 1994, pp. 206–209.
[5] S. Wiedeman, J. Kessler, T. Lommasson, L. Russell, J. Fogelbach, S. Skibo, R. Arya, D. Carlson, Optimization of Cu(In,Ga)Se_2 photovoltaic modules, Proc. 13th European Photovoltaic Solar Energy Conf., 1995, to be published.
[6] R.J. Matson, K.A. Emery, I.L. Eisgruber, L.L. Kazmerski, The large-scale laser scanner: milli-characterization of photovoltaic devices and modules, Proc. 12th European Photovoltaic Solar Energy Conf. Exhibition, 1994, pp. 1222–1225.
[7] J.L. Gray, ADEPT: A general purpose numerical device simulator for modeling solar cells in one, two, and three dimensions, Proc. 22nd IEEE Photovoltaics Specialists Conf., 1991, pp. 436–438.
[8] P.J. McElhany, J.K. Arch, H.S. Lin, S.J. Fonash, J. Appl. Phys. 64 (3) (1988) 1254.
[9] I.L. Eisgruber, R.J. Matson, J.R. Sites, K.A. Emery, Interpretation of laser scans from thin-film polycrystalline photovoltaic modules, Proc. 1st World Conf. on Photovoltaic Energy Conversion, 1994, pp. 283–286.
[10] P.H. Mauk, H. Tavakolian, J.R. Sites, Interpretation of thin-film polycrystalline solar cell capacitance, IEEE Trans. Electron Dev. 37 (2) (1990) 422.
[11] D. Schmid, M. Ruckh, H. Schock, A Comprehensive Characterization of the Interfaces in Mo/CIS/CdS/ZnO Solar Cell Structures, Proc. 1st World Conf. on Photovoltaic Energy Conversion, 1994, pp. 198–201.
[12] S.H. Wei, A. Zunger, Appl. Phys. Lett. 63 (1993) 2549.